EAST EUROPEAN JOURNAL OF PHYSICS. 3. 689-702 (2026)
DOI:10.26565/2312-4334-2026-3-65 ISSN 2312-4334

NONDESTRUCTIVE ULTRASONIC EVALUATION OF TEMPERATURE-DEPENDENT MECHANICAL AND ELASTIC PROPERTIES OF PbX (X = S, Se) COMPOUNDS

Sudhanshu Tripathi[1], Praveen Singh[2], Anurag Singh[2,3], Devraj Singh[2], R. Khenata[4,5*], M. Boudjelal[4], H. Meradji[6], Ajit Kumar Maddheshiya[7], Shanay Rab[8], M. Faizan[9], S. Bin-Omran[10]**

[1]Amity Institute of Information Technology, Amity University, Sector-125, Noida – 201313, U.P., India
[2]Department of Physics, Prof. Rajendra Singh (Rajju Bhaiya) Institute of Physical Sciences for Study and Research, Veer Bahadur Singh Purvanchal University, Jaunpur-222003, U.P., India
[3]Department of Physics, Government Degree College, Babhani, Sonbhadra-231208, U.P., India
[4]Laboratoire de Physique Quantique de la matière et de Modelisation Mathematique (LPQ3M), Universite de Mascara, Mascara, 29000, Algeria
[5]Algerian Academy of Sciences & Technologies, 04- Path of Peace, Hydra- Algiers16000, Algeria
[6]Laboratoire LPR, Département de Physique, Faculté des Sciences, Université Badji Mokhtar, Annaba, Algeria
[7]Department of Physics, University of Allahabad, Prayagraj-211002, India
[8]School of Architecture, Technology and Engineering, University of Brighton, BN24AT, UK
[9]School of Materials Science and Engineering, Jilin University, Changchun, 130012, China
[10]Department of Physics and Astronomy, College of Science, King Saud University, P.O. Box 2455, Riyadh, 11451, Saudi Arabia
**Corresponding Author email: khenata_rabah@yahoo.fr; rabah_khenata@univ-mascara.dz; **Email: somran@ksu.edu.sa*
Received April 16, 2026; revised July 29, 2026; accepted August 2, 2026

A comprehensive investigation of the elastic, mechanical, and thermo-acoustic properties of lead monochalcogenides PbX (X = S, Se) has been carried out along the principal crystallographic directions ⟨100⟩, ⟨110⟩ and ⟨111⟩ within the temperature range of 0-300 K using the ultrasonic non-destructive evaluation method. The second- and third-order elastic constants (SOECs and TOECs) were computed using the Coulomb and Born–Mayer potential frameworks, confirming the elastic stability of the materials under study. Derived mechanical parameters and ultrasonic velocities were obtained from SOECs, indicating brittle mechanical behavior based on Pugh's ratio. At 300 K, the Debye temperature, Debye velocity, lattice thermal conductivity, acoustic nonlinearity parameter, and ultrasonic attenuation coefficient were evaluated along the studied orientations. Among all the directions, the ⟨111⟩ orientation exhibited the highest Debye temperature and Debye velocity. The dominant mechanism of ultrasonic attenuation was identified as Akhiezer-type, emphasizing its relevance in thermal dissipation and acoustic damping. The findings suggest that PbSe possesses superior elastic stiffness, whereas PbS exhibits enhanced thermal conductivity and stronger phonon interactions. These characteristics underscore the potential of PbS and PbSe for applications in thermoelectric and ultrasonic sensing technologies.
Keywords: *Lead monochalcogenides; Elastic properties; Mechanical constants; Thermal conductivity; Ultrasonic attenuation*

1. INTRODUCTION

To meet the growing global demand for energy, researchers are increasingly focusing on renewable energy sources, including solar energy, biofuels, wind energy, thermoelectric power, and fuel cells. Among the materials explored for these applications, lead-based chalcogenides, especially lead sulfide (PbS) and lead selenide (PbSe), have gained significant recognition in both fundamental research and practical applications due to their distinctive properties [1]. In terms of theoretical and experimental studies, the work of Zhang et al. [2] has provided important insights into the anharmonic properties of lead chalcogenides. Using density functional theory (DFT) and first-principles calculations, their research elucidates the complex interplay between phonon interactions and thermal transport properties in these materials. This foundational work underscores the importance of a detailed understanding of both the electronic and photonic contributions to the overall performance of thermoelectric materials. These materials are important in a variety of high-technology applications, including thermoelectric devices, infrared detectors, and photovoltaic cells [3]. The unique properties of PbX (X: S,Se), such as their narrow bandgap, high carrier mobility, and low thermal conductivity, make them ideal candidates for these applications [4]. Kang and Wise [5] also studied the optical properties and electronic structure of lead sulfide and lead selenide quantum dots. The elastic properties of PbX materials are crucial for understanding their mechanical stability and potential for device integration. Tripathi et al. [6] have investigated the non-linear elastic and acoustic properties of PbTe and found that the ultrasonic attenuation is lowest at 100K which is a highly stable condition. Thermophysical properties, including thermal expansion and thermal conductivity, are equally important for applications where thermal management is crucial. PbS and PbSe exhibit interesting thermal behavior, which is essential for optimizing their performance in thermoelectric applications [7]. Studies have shown that ultrasonic attenuation in chalcogenide materials varies with temperature and frequency, providing the potential for their use in temperature-sensitive

Cite as: S. Tripathi, P. Singh, A. Singh, D. Singh, R. Khenata, M. Boudjelal, H. Meradji, A.K. Maddheshiya, S. Rab, M. Faizan, S. Bin-Omran, East Eur. J. Phys. 3, 689 (2026), https://doi.org/10.26565/2312-4334-2026-3-65

applications [8]. Recent advances in the study of lead chalcogenides have provided even greater insight into their thermal, mechanical, and electronic properties. Skelton et al. [9] carried out first-principles investigations into the thermophysical properties of PbX, focusing on their lattice dynamics and temperature-dependent behaviour. Their study provided important insights into phonon softening, a phenomenon crucial for understanding the temperature dependence of thermal conductivity, which has a major impact on the thermoelectric performance of these materials. By modeling phonon-phonon interactions, the research highlights the ability of PbSe and PbTe to maintain high thermoelectric performance at high temperatures. Anwar et al. [10] explored the influence of synthesis conditions, particularly the bath temperature, on the structural and thermoelectric properties of PbSe thin films. The study found that higher temperatures during chemical bath deposition improved the crystallinity and particle size of the PbSe films, leading to better thermoelectric performance. This finding underscores the importance of controlled synthesis processes in optimizing the functional properties of PbSe for practical applications in energy conversion technologies. Chen et al. [11] demonstrated that the synthesis medium directly affects the size and morphology of PbSe nanostructures, with nanorods exhibiting superior electrochemical properties compared to other morphologies. The study also highlights the importance of structural stability in nanostructures for energy storage and conversion applications, demonstrating that smaller nanostructures exhibit better electrochemical performance, thereby further strengthening the role of PbSe in next-generation energy technologies. Jahromi and Moaddeli [12] used density functional theory to study the band structure of PbS, revealing its potential for ultraviolet photoconductive devices. The study highlights the wide applicability of PbS, which has traditionally been used in infrared technologies but is now being considered for ultraviolet applications as well, highlighting its versatility. Abe [13] observed phase transformations between PbS and PbSe during thin-film deposition, revealing significant changes in the crystalline structure that affect the material's optical properties. This transformation from PbS to PbSe during film deposition suggests new possibilities for tuning the material's properties through controlled synthesis. As studied by Bandoh et al. [14], annealing of PbSe films improved both optical and structural properties, increasing crystallite size and reducing lattice defects. This improvement in material quality translates into enhanced performance in optoelectronic devices, where crystal structure and purity are crucial to the device's efficiency. Nanocrystalline PbS thin films, as investigated by Bayisa et al. [15], were also shown to exhibit excellent optical and structural properties, with the size of the crystallites increasing as the film thickness was varied. These findings suggest that controlling the film thickness during deposition can improve the material properties, thereby enhancing the performance of PbS-based devices. Recent research has also focused on developing PbSe-based multifunctional devices. Khusayfan et al. [16] successfully produced PbSe thin films for use in photovoltaic devices, microwave resonators, and X-ray sensors. Their work highlighted the adaptability of PbSe for various high-tech applications, especially wireless communication technologies such as 5G. The structural and optical properties of PbSe thin films make them ideal for use in next-generation devices, demonstrating the material's versatility. Yang et al. [17] developed a novel electrochemical synthesis method to fabricate hierarchically porous PbSe films, which showed excellent infrared photodetection properties. These porous structures provide a large surface area, thereby improving the material's photoconductive sensitivity and making it highly effective for infrared detection at room temperature. This advancement opens new doors for the use of PbSe in low-cost, high-performance photodetectors.

The limited exploration of ultrasonic attenuation in PbX compounds motivated a detailed investigation employing ultrasonic non-destructive evaluation techniques. This study presents a systematic analysis of the anisotropic and temperature-dependent elastic, mechanical, thermal, and acoustic properties of PbX (X = S, Se) across principal crystallographic directions and within the temperature range of 0–300 K. The results provide critical insights into the behavior of these materials under varying thermal and structural conditions, emphasizing their potential relevance in industrial and functional applications. The calculated parameters are benchmarked against established data to validate the reliability of the theoretical framework, which is grounded in the Born–Mayer interaction potential model.

2. COMPUTATIONAL APPROACH

2.1 Nonlinear Elastic Behavior: SOECs and TOECs

SOEC and TOEC serve as important links between mechanical properties and dynamic behavior in crystalline materials. We have estimated the temperature-dependent SOECs and TOECs using the methodology proposed by Brugger [18]. The potential used to evaluate these elastic constants is obtained by combining the electrostatic and repulsive potentials.

$$F\ (\mathrm{r}) = F^{C}(\mathrm{r}) + F^{B}(\mathrm{r}). \tag{1}$$

The Born Mayer / repulsive potential, $F^{C}(\mathrm{r})$ and $F^{B}(r)$ are prearranged as

$$F^{C}(r) = \pm\left(\frac{e^{2}}{r}\right) \text{ and } F^{B}(r) = Aexp\left(\frac{-r}{b}\right). \tag{2}$$

Here, b characterizes the stiffness parameter, r denotes the distance between nearest-neighbour atoms, e refers to the electronic charge, and A corresponds to the interaction strength factor [18].

The lattice dynamics framework has been proposed by Leibfried and Ludwig [19], Ghate [20], Mori and Hiki [21] and the lattice energy is found to vary with temperature. Combining the static and vibrational part SOECs and TOECs ($C_{ij}$and C_{ijk}) can be defined as

$$C_{ij} = C_{ij}^{0} + C_{ij}^{vib} \quad \text{and} \quad C_{ijk} = C_{ijk}^{0} + C_{ijk}^{vib} \tag{3}$$

Here, the superscript '*vib*' indicates the vibrational component of SOECs and TOECs at elevated temperature and '*0*' depicts the static component at 0K. The formulae for computing the C_{ij} and C_{ijk} are given in literature [22].

2.2 Mechanical Parameters

The SOECs were used to estimate the mechanical parameters [23] like bulk modulus (B), shear modulus (G), Young's modulus (E), Tetragonal modulus (Cs), shear modulus (G), Cauchy pressure (C_P), Zener anisotropic factor (Z_A), Pugh's indicator (B/G) and Poisson's ratio (ν) [23] and their values are placed in Table 1.

Table 1. The formulae for the mechanical parameters of PbX

$B = \frac{(C_{11}+C_{12})}{3}$	$G = \frac{(C_{11}-C_{12}+3C_{44})}{10} + \frac{2.5(C_{11}-C_{12})C_{44}}{4[C_{44}+3(C_{11}-C_{12})]}$
$E = \frac{9GB}{G+3B}$	$Cs = \frac{C_{11}-C_{12}}{2}$; $C_p = C_{12} - C_{44}$
$Z_A = \frac{2C_{44}}{C_{11}-C_{12}}$	$\nu = \frac{3B-2G}{6B+2G}$

2.3 The Nonlinearity Parameter

The transmission of ultrasonic waves through a solid medium leads to waveform distortion, primarily influenced by the material's microstructural features. The acoustic nonlinearity parameter quantifies this effect and is defined as the negative ratio of the nonlinear to the linear terms in the finite-amplitude longitudinal wave equation, evaluated along various crystallographic directions. Breazeale's nonlinearity constant, which captures this behavior, is expressed as a linear combination SOECs and TOECs, and is given by:

$$\beta = -(3K_2 + K_3)/K_2$$

where K_2 and K_3 depends on SOECs and TOECs. The detailed expression of K_2 and K_3 are described in literature [6].

2.4 Direction-Dependent Ultrasonic Velocities

The three modes of ultrasonic wave velocities described due to ultrasonic wave propagation are namely one longitudinal (V_L), and two transverse modes namely quasi-shear (V_{S2}) and shear (V_{S1}) velocities respectively, propagating along different crystallographic orientations [24]. Due to crystal symmetry, the two shear modes degenerate along $\langle 100 \rangle$ and $\langle 111 \rangle$ directions, polarised along $\langle 100 \rangle, \langle 001 \rangle, \langle 1\bar{1}0 \rangle$ and $\langle \bar{1}10 \rangle$ planes. The formulae for these velocities are described in literature [24]. The average of these velocities defined at Debye average velocity (V_D) given as

$$V_D = \left[\frac{1}{3}\left\{\frac{1}{{V_L}^3} + \frac{1}{{V_{S1}}^3} + \frac{1}{{V_{S2}}^3}\right\}\right]^{-\frac{1}{3}} \tag{4}$$

2.5 Thermoacoustic Properties

Another important parameter that describes the material thermophysical characteristics is Debye temperature (θ_D) which depends on material parameters and Debye velocity [25] given as

$$\theta_D = \frac{h}{k_B}\left(\frac{3nN\rho}{4\pi M}\right)^{\frac{1}{3}} V_D \tag{5}$$

Where h, k_B, n, N, ρ, M and V_D are Planck constant, Boltzmann constant, number of atoms per unit cell, Avogadro number, density of substance, molecular weight of substance and Debye average velocity, respectively.

The thermal conductivity κ is directly influenced by Debye temperature θ_D [26] given as

$$\kappa = \frac{AM\delta T_D^3 n^{1/3}}{\gamma^2 T} \tag{6}$$

Where A = 3.04×10^{-8}; M is defined as average atomic mass in amu; δ (in Å) is the cube root of volume per atom; γ is the Grüneisen parameter calculated in different directions of ultrasonic wave propagation within the temperature regime 0-300K.

Thermal relaxation time τ_{th} [27] determined as the time taken by phonon particles to regain thermal equilibrium given as

$$\tau_{th} = \frac{1}{2}\tau_L = \tau_S = \frac{3\kappa}{C_V V_D^2} \tag{7}$$

Where C_V represents the specific heat at constant volume, calculated with the help of the AIP Handbook [28]. The transformation of thermal to acoustic energy defined as the acoustic coupling constant [29] is given as

$$D = 9\langle (\gamma_i^j)^2 \rangle - \frac{3\langle \gamma_i^j \rangle^2 \rho c_V T}{E_0} \tag{8}$$

The propagation of ultrasonic waves through matter can be used to provide details about it. The details provided by the wave are related to amplitude and phase, yet they can be interpreted to reveal many features within matter. When

ultrasonic waves are generated and propagate within a material, energy is lost due to scattering, absorption, and the difference in acoustic impedance of two different materials at their interface [30].

The factors affecting the ultrasonic attenuation coefficient in an ideal crystal are thermoelastic relaxation mechanism (TRM), phonon-phonon interaction (PPI), and electron-phonon interaction (EPI). The thermal attenuation caused during the maintenance of the equilibrium process for the transfer of energy between compressed and rarefied region when the ultrasonic wave passes through the crystal [31,32], defined as

$$\left(\frac{\alpha}{\nu^2}\right)_{\text{th}} = \frac{4\pi^2 < \gamma_i^j >^2 kT}{2\rho V_L^5}. \tag{9}$$

The ultrasonic attenuation resulting from p-p interactions, applicable to both longitudinal and shear waves under defined conditions, is given as follows: $\omega\tau \ll 1$ (where τ denotes the thermal relaxation time and ω represents the angular frequency) is [33].

$$\left(\frac{\alpha}{\nu^2}\right)_l = \frac{4\pi^2 \tau_{th} E_0 \, (D_L/3)}{2\rho V_L^3}. \tag{10}$$

$$\left(\frac{\alpha}{\nu^2}\right)_s = \frac{4\pi^2 \tau_{th} E_0 \, (D_S/3)}{2\rho V_S^3}. \tag{11}$$

Here E_0 represents the thermal energy density obtained from the AIP handbook, while V_L and V_S represent the velocities for the longitudinal and shear modes of propagation, respectively.

3. RESULTS AND DISCUSSION

The SOECs and TOECs for PbS and PbSe in the temperature range of 0 to 300 K are evaluated using the lattice parameter obtained from literature [2,34] and hardness parameters (b = 0.303Å) for PbS and PbSe [35]. The SOECs and TOECs are affected by both the anharmonic lattice vibrations and thermal expansion coefficient [36]. The obtained values of SOECs and TOECs for PbX are listed in Table 2.

Table 2. SOECs and TOECs of PbX [in (GPa)]

Temp. (K)	Material	C_{11}	C_{12}	C_{44}	C_{111}	C_{112}	C_{123}	C_{144}	C_{166}	C_{456}
0		93.92	11.28	11.28	-1198.5	-39.05	16.84	16.84	-39.05	16.84
50		97.66	10.80	10.90	-2022.3	-37.18	14.31	16.88	-39.16	16.84
100		98.56	10.33	10.86	-2021.5	-35.59	11.77	16.85	-38.98	16.84
150		99.93	9.83	10.82	-2026.2	-33.81	9.20	16.83	-38.82	16.84
200	PbS	101.39	9.32	10.76	-2032.1	-31.96	6.61	16.78	-38.86	16.84
300		104.43	8.30	10.64	-2045.7	-28.22	1.42	16.68	-38.20	16.84
0		100.86	13.08	13.08	-2089.8	-45.53	19.29	19.29	-45.53	19.29
50		103.89	12.61	12.64	-2116.4	-43.85	16.82	19.34	-45.63	19.29
100	PbSe	105.19	12.10	12.60	-2119.7	-42.11	14.28	19.32	-45.46	19.29
150		106.71	11.57	12.54	-2125.8	-40.24	11.71	19.28	-45.25	19.29
200		108.29	11.03	12.48	-2132.7	-38.33	9.13	19.22	-45.01	19.29
300		111.34	9.92	12.30	-2145.1	-34.36	3.89	19.05	-44.37	19.29

As shown in Table 2, the longitudinal elastic constant C_{11} increases with temperature, while the compression coefficient C_{12} and elastic constant C_{44} decrease with increasing temperature. The elastic constant C_{44}, which is responsible for the shear modulus perpendicular to the applied stress, is slightly decreasing with temperature. From the increasing C_{11} and decreasing C_{12}, C_{44}, it can be inferred that the selected PbX becomes stiffer and softer at higher temperatures. Cauchy's criterion for isotropic cubic crystals is derived from the assumption that the internal forces of the material are perfectly central and the material is stress free. The Cauchy criteria $C_{12}^0 = C_{14}^0$, $C_{112}^0 = C_{166}^0$, $C_{123}^0 = C_{144}^0 = C_{456}^0$. [37] proposed by Cousin [38] are valid at absolute 0K, for PbS and PbSe but fail at higher temperatures, which implies that at 0K the interaction forces are central but have increasing ionic character as the temperature increases. The TOECs estimated using the theory proposed by Brugger [18] and are utilized to analyze the acoustical and thermal phonon interactions and other anharmonic properties of the material under examination. It is obvious from Table 2 that the magnitude of C_{111} is decreasing with increasing temperature, while the magnitude of C_{112}, C_{123} and C_{166} are increasing with temperature. The elastic constant C_{144} is nearly constant due to the small effect of the vibrational part, while C_{456} is constant at every temperature due to the absence of vibrational energy. The TOECs pattern of PbX (X: S,Se) are similar to that of lead telluride [6] and tin monochalcogenides [38].

Figure 1 depicts the deviation plot for SOECs of the present work with previously reported values by experimental and theoretical methods [2, 39, 40]. The variation of SOECs obtained in the present work relative to previously reported values in the literature is ≈ ±10%, due to differences in the computational approach. The observed variations in elastic constants as depicted in Fig. 1, with previously reported values are due to their dependency on temperature-dependent lattice parameters, anharmonic phonon contribution and thermal expansion effect which is linked through the Grüneisen

parameters which connect the mechanical (elastic) and thermal properties of a crystalline solid. The elastic constants at elevated temperatures can be attributed to the increased contribution of vibrational energy. This implies that, with rising temperature, atomic interactions and the corresponding interaction potentials within the crystal lattice are modified due to the influence of non-central forces. Consequently, a comprehensive understanding of the temperature dependence of elastic constants is essential for accurately predicting the effects of thermal conditions on a material's mechanical strength, stiffness, and the interatomic force dynamics across adjacent crystallographic planes. The Born stability criterion,$\{[(C_{11}+2C_{12})/3]>0;\ C_{44}>0;\ [(C_{11}-C_{12})/3]>0\}$is satisfactorily fulfilled by the obtained values of elastic constants.

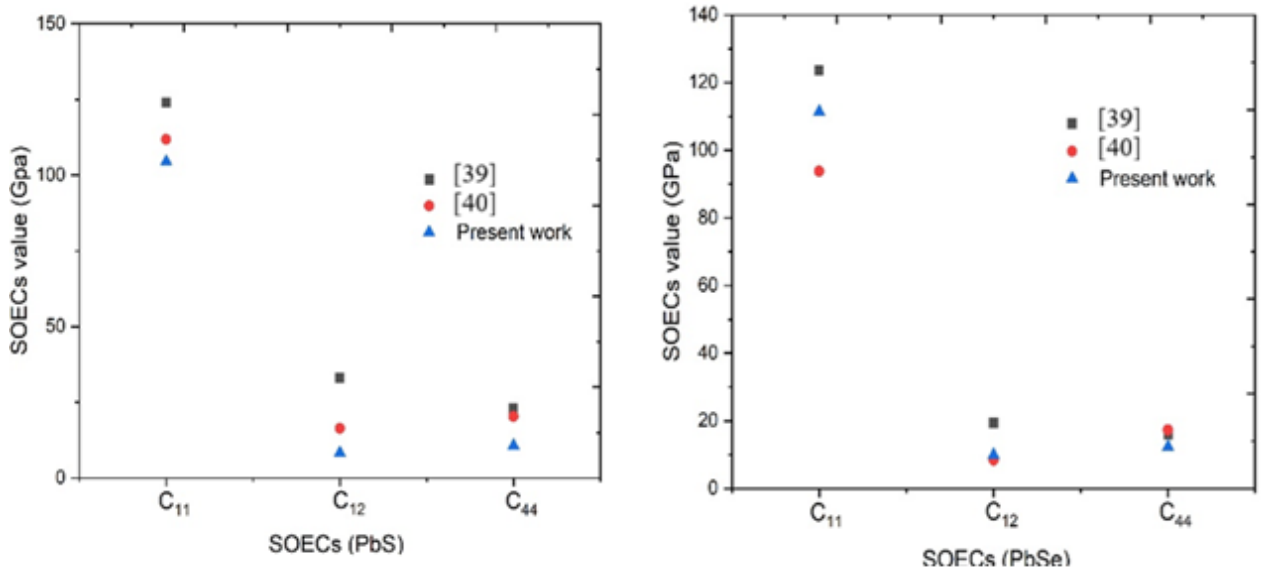

Figure 1. Deviation plot for SOECs of PbS and PbSe

Therefore, while PbX (X: S,Se) is confirmed to be mechanically stable under the Born criterion, it remains imperative to analyze the evolution of its mechanical parameters with temperature to assess its suitability for high-temperature applications. To analyze the mechanical properties of PbX (X: S, Se), various mechanical parameters are calculated for PbS and PbSe using the expressions defined in Table 1, within the temperature regime 0–300K and are depicted in Table 3.

Table 3. The mechanical parameters of PbX (X; S,Se)

Material	Temp. (K)	*E* (GPa)	*B* (GPa)	*B** (GPa)	*G* (GPa)	*B/G*	Z_A	*ν*	*Hv*	C_P (GPa)	C_S (GPa)
PbS	0	50.34	38.83	54.6	19.60	1.66	0.27	0.28	3.27	0	41.32
	50	50.82	39.75	53.6	19.74	1.66	0.26	0.28	3.31	-0.10	43.43
	100	51.06	39.74	51.6	19.85	1.64	0.25	0.28	3.41	-0.53	44.16
	150	51.46	39.86	49.5	20.02	1.62	0.24	0.28	3.53	-0.98	45.04
	200	51.86	40.04	47.2	20.19	1.60	0.23	0.28	3.65	-1.43	46.03
	300	52.67	40.34	42.3	20.53	1.57	0.22	0.28	3.88	-2.34	48.06
PbSe	0	55.81	42.34	48.4	21.79	1.66	0.29	0.28	3.67	0	43.88
	50	55.99	43.04	47.6	21.82	1.66	0.28	0.28	3.68	-0.03	45.64
	100	56.38	43.13	46.2	21.98	1.64	0.27	0.28	3.79	-0.49	46.53
	150	56.81	43.28	44.7	22.16	1.63	0.26	0.28	3.91	-0.96	47.56
	200	57.23	43.45	43.1	22.34	1.61	0.25	0.28	4.03	-1.44	48.62
	300	57.96	43.73	39.9	22.65	1.58	0.24	0.27	4.26	-2.37	50.71

*Ref [2]

As depicted in Table 3, Young's modulus, responsible for the stiffness of the material, is increasing with an increase in temperature for PbX (X: S, Se), and the value of for PbSe is higher than PbS. Thus, PbSe is stiffer than PbS, which is highest at 300 K. The obtained values of *E* for PbX (X: S, Se) are nearly similar to those reported by Seetawan et al. [41] at 300 K using the molecular dynamics method. The bulk modulus indicates a material's resistance to changes in volume. PbS is more compressible than PbSe, which is highest at 300 K for PbX. The reported values of *B* for PbS are 62.8 GPa by experimental method [39] and equal 55.7 GPa and 65.6 GPa, calculated by GGA and LDA methods [2], respectively. As depicted in Table 3, the estimated value of *B* in the present work at 300 K is 40.34 GPa, indicating deviations of 5.4% to 19% due to differences in the approach used.

Modulus of rigidity (*G*) represents the behaviour of the material to resist change in size and shape. In the present study, *G* values increase with increasing temperature for selected PbX (X: S, Se). As the reported values of *Cs* and

Shear modulus for PbSe are higher than those of PbS at 300K, as depicted in Table 3, it indicates that PbSe is stiffer and harder than PbS, as it resists deformation more under both shear and elastic distortions. A similar result has been reported by Seetawan et al. [41] at elevated temperatures, which justifies our approach.

Pugh's index (B/G) compares fracture to toughness which measures the ductility and brittleness of materials. If the Pugh index is more than 1.75, then the selected compound is ductile; otherwise, it is brittle. It is evident from Table 3 that Pugh's ratio for both PbS and PbSe is less than 1.75, indicating that both materials are brittle at all temperatures examined in the present work. Poisson's ratio is an important variable for defining the behavior of intermolecular forces. The relation $0.5>\nu>0.2$ is valid for non-central forces and ionic values are around 0.25. In the present case as Table 3 shows, values are approximately 0.28 which satisfy the relation of non-central. Thus, the ν values predict that the inter-atomic forces are non-central and ionic in nature. For brittle materials, the Cauchy pressure is $Cp=(C_{12}-C_{44})$ <0 and the Poisson ratio is $\nu < 0.3$. Table 3 shows that Cp <0 and ν <0.3, which predicts that PbS and PbSe are brittle in nature, which validates our previous prediction (on the basis of Pugh's index) of the brittle nature of both materials in the present investigation. The Zener anisotropy index (Z_A) is a dimensionless quantity that measures the isotropy of a cubic crystal. For isotropic materials Z_A value is equal to 1. Table 3 shows that the Zener index is different from 1, which indicates that the selected PbX are anisotropic in the temperature range 0-300 K. Figure 2 presents the combined plot of the Cauchy pressure Cp/Y versus the G/B ratio for PbX (X: S, Se) over the temperature range of 0–300 K. The observed downward trend toward the lower right corner of the plot is attributed to the directional nature of bonding in the material, which promotes brittle behaviour, revealing the anticipated mechanical response based on theoretical predictions.

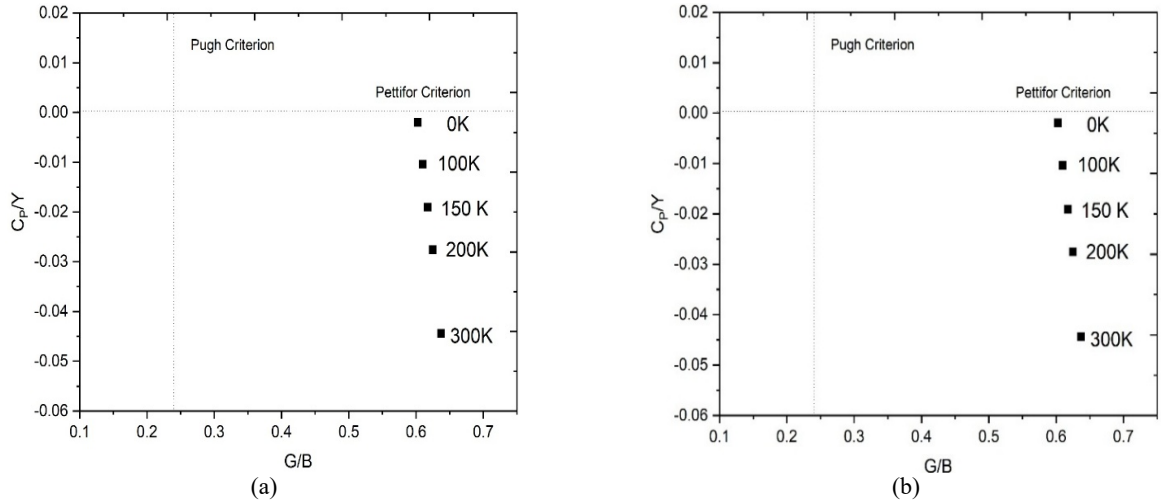

Figure 2. Renormalized Pugh and Pettifor criteria for (a) PbS, (b) PbSe within the temperature range 0-300K

The estimated SOECs and TOECs were utilized to compute the nonlinearity parameters $K2$ and $K3$ [6], which are subsequently used to evaluate the temperature-dependent Breazeale's nonlinearity parameter β across the temperature range of 0–300 K. The variation of β along different principal directions of wave propagation is illustrated in Fig. 3, highlighting the anisotropic nonlinear elastic behavior of PbX (X:S,Se) with respect to temperature.

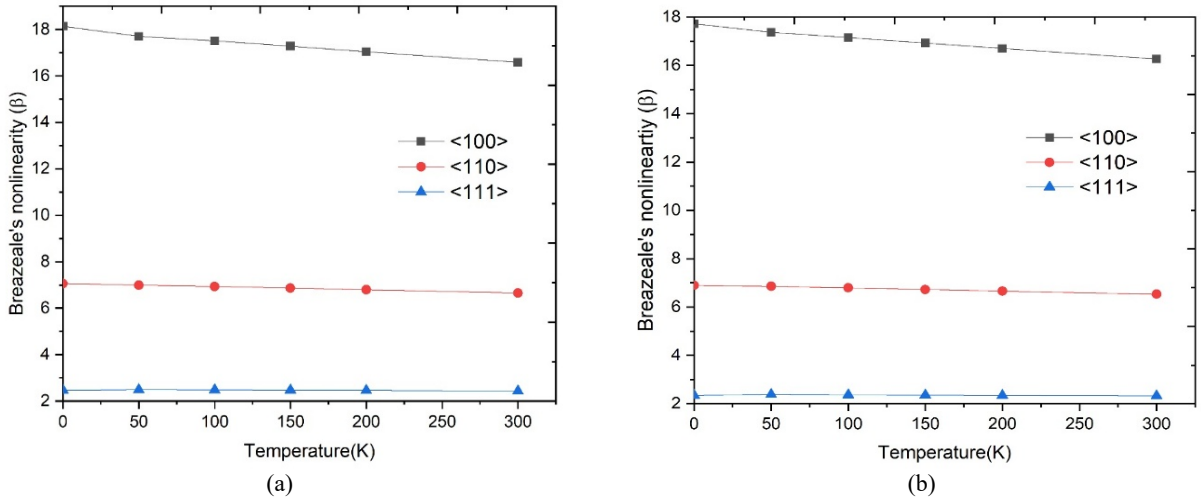

Figure 3. Orientation-dependent Breazeale's nonlinearity constant with temperature (a) PbS (b) (PbSe)

Figure 3 reveals that the maximum value of the nonlinearity parameter β is observed along the ⟨100⟩ crystallographic direction, while the minimum value is recorded along the ⟨111⟩ direction. Furthermore, it is evident that the nonlinear parameter β for PbX (X= S, Se) does not exhibit a consistent trend with increasing temperature, indicating a complex dependence on thermal effects. The nonlinearity parameter β does not remain uniform across different crystallographic orientations; however, a general linear decreasing trend in its value is observed as the temperature increases. Ultrasonic velocity measurements are employed to gain insights into the microstructural characteristics of the material.

To validate and extend our calculations, 3D visualizations showing the directional dependence of Young's modulus (E), bulk modulus (B), and shear modulus (G) are presented in Figs. 4,5, and 6 respectively. These visualizations also include their 2D projections on the (100), (010) and (001) planes. The calculations for B and G are based on established relations given in the literature [42], while the values of G are further elaborated using references from the literature [43].

$$\frac{1}{B} = (S_{11} + 2S_{12})(l_1^2 + l_2^2 + l_3^2) \tag{12}$$

$$\frac{1}{E} = S_{11} - 2\left(S_{11} - S_{12} - \frac{1}{2}S_{44}\right)(l_1^2 l_2^2 + l_2^2 l_3^2 + l_3^2 l_1^2) \tag{13}$$

$$\frac{1}{G} = S_{44} - 4\left(S_{11} - S_{12} - \frac{1}{2}S_{44}\right)(\sin^2\theta\cos^2\theta + 0.125\sin^4\theta)(1 - \cos 4\varphi) \tag{14}$$

Here, $S_{ij} = C_{ij}^{-1}$ denotes the elastic compliance matrix, which is obtained as the inverse of the elastic constant matrix. The terms l_1, l_2, and l3 denote the 3D directional cosines corresponding to the x-, y-, and z-axes, respectively.

A material is classified as isotropic if its 3D and 2D plots exhibit spherical and circular symmetries, respectively; deviation from these symmetries indicates anisotropy. As shown in Figs. 4, 5, and 6, the bulk modulus exhibits isotropic behavior, maintaining consistent spherical symmetry in its 3D representation. In contrast, both Young's modulus (E) and shear modulus (G) deviate significantly from spherical symmetry in their 3D diagrams and from circular symmetry in their 2D projections, highlighting their inherent anisotropic properties.

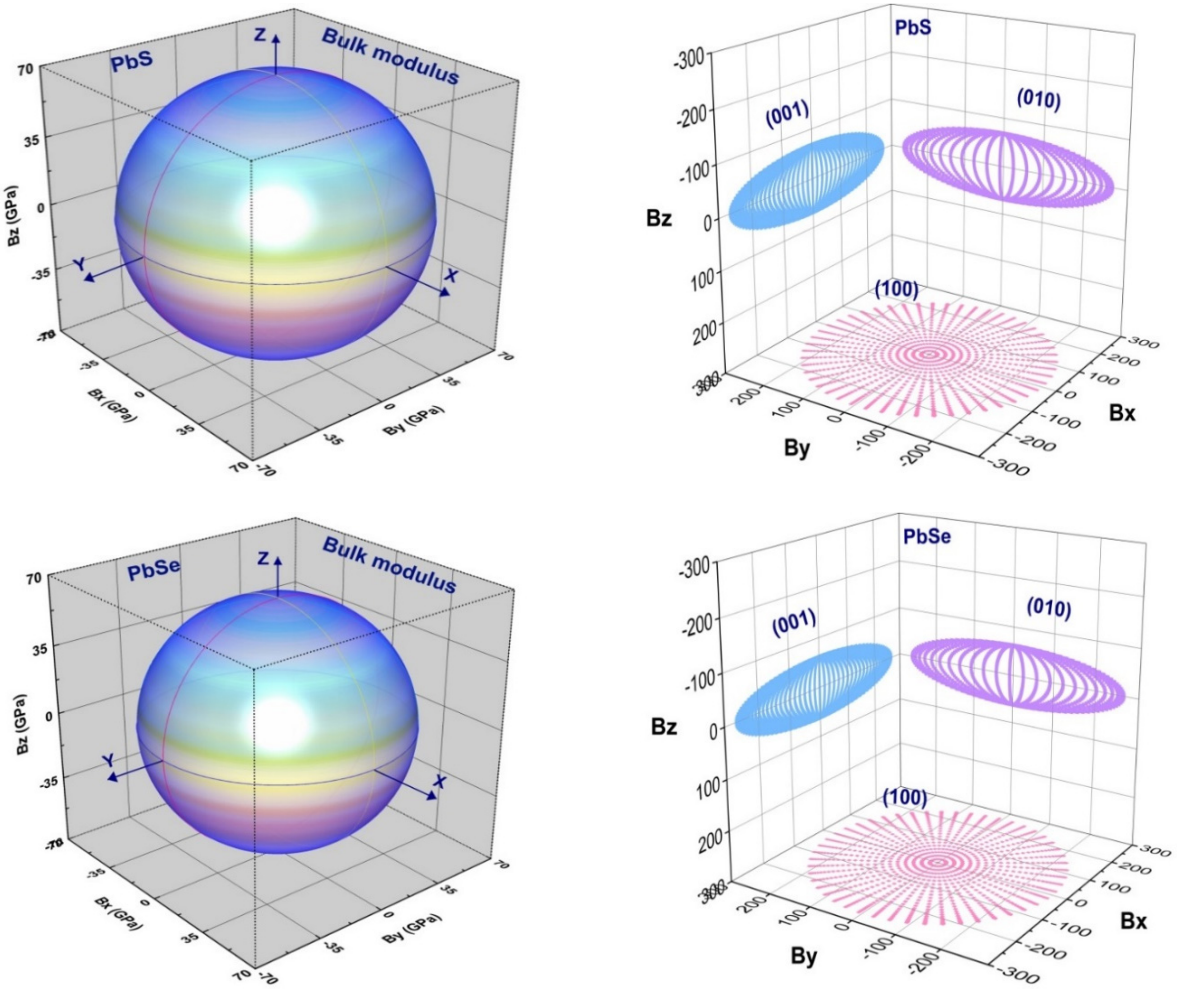

Figure 4. 3D-directional dependence of the bulk modulus (B, in GPa) for PbX and its projection in dissimilar planes

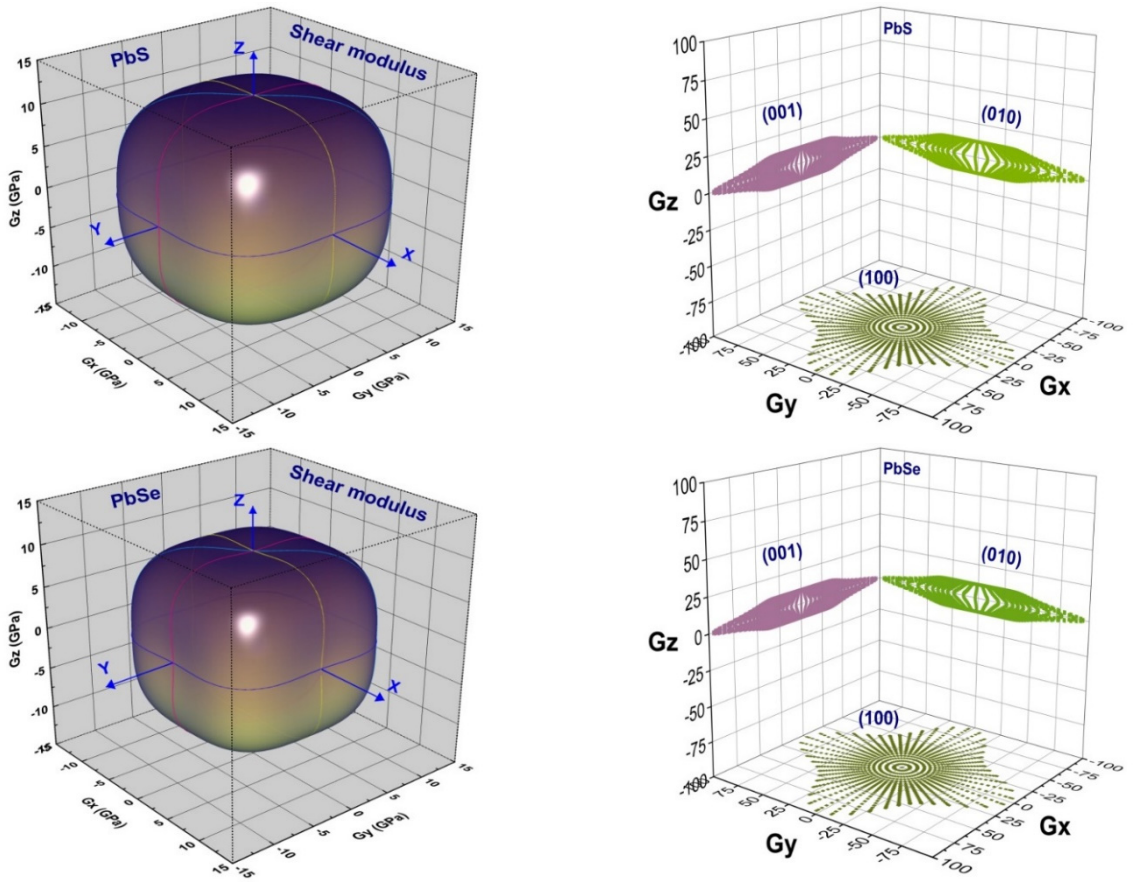

Figure 5. 3D-directional dependence of the shear modulus (*G*, in GPa) and its projections in dissimilar planes for PbX

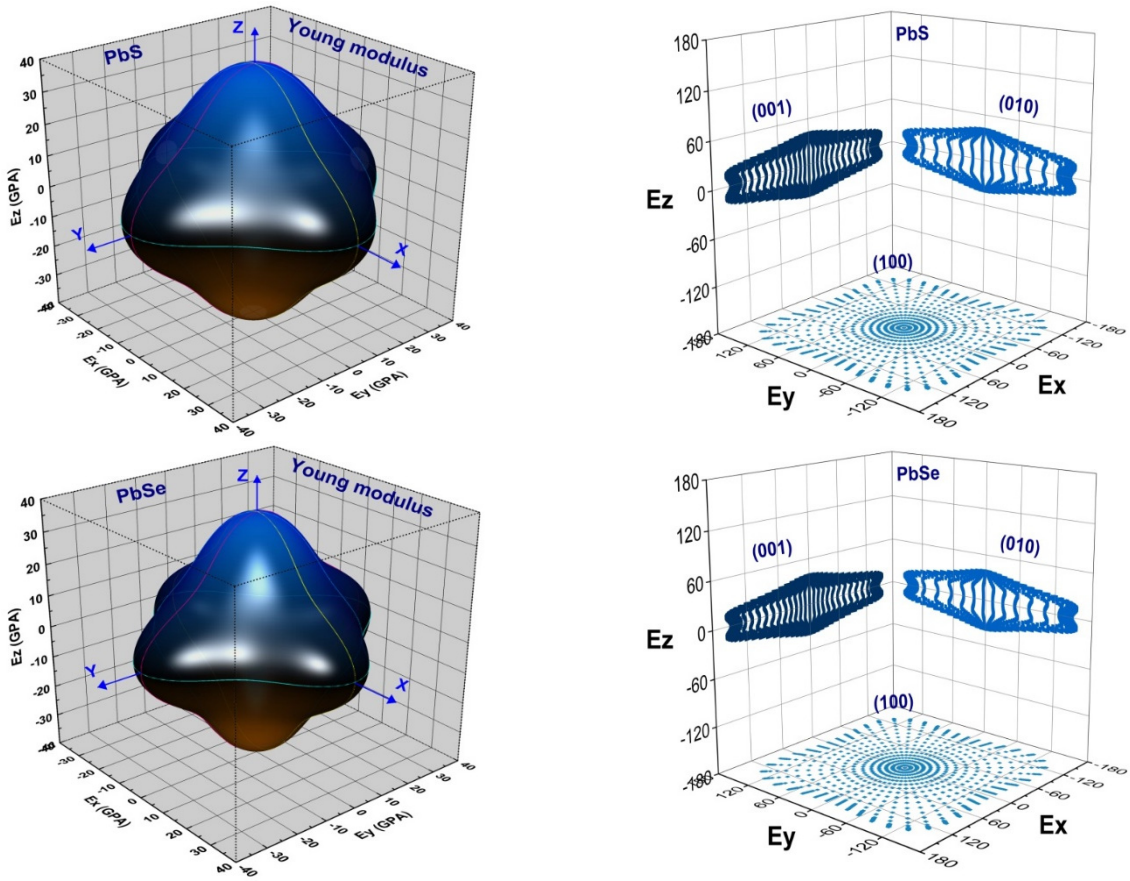

Figure 6. 3D-directional dependence of the Young's modulus (*E*, in GPa) and its projections in dissimilar planes for PbX

Ultrasonic velocity provides information about the microstructure, texture, and damage in materials [44]. The temperature-dependent ultrasonic velocities e.g., longitudinal ultrasonic velocity, shear ultrasonic velocity and quasi-shear ultrasonic velocity along the $\langle 100\rangle, \langle 110\rangle$and $\langle 111\rangle$ direction, with the direction of polarization along $\langle 100\rangle, \langle 001\rangle, \langle 1\bar{1}0\rangle$ and $\langle \bar{1}10\rangle$ are evaluated using SOECs and densities of PbX in the temperature range 0 - 300K are depicted in Table 4.

Table 4. Ultrasonic velocities (in 10^3m/s) of PbS and PbSe

Orientation	Temp.	PbS				PbSe			
	(K)	V_L	V_{S1}	V_{S2}	V_D	V_L	V_{S1}	V_{S2}	V_D
$\langle 100\rangle$	0	3.5107	1.2169	1.2169	1.3840	3.5255	1.2698	1.2698	1.4429
	50	3.5789	1.1964	1.1964	1.3616	3.5782	1.2485	1.2485	1.4197
	100	3.5963	1.1939	1.1939	1.3589	3.6003	1.2464	1.2464	1.4175
	150	3.6212	1.1916	1.1916	1.3565	3.6264	1.2435	1.2435	1.4104
	200	3.6475	1.1885	1.1885	1.3532	3.6531	1.2401	1.2401	1.4109
	300	3.7018	1.1820	1.1820	1.3462	3.7043	1.2313	1.2313	1.4015
$\langle 110\rangle$	0	2.8955	1.2169	3.2930	1.6883	2.9382	1.2698	3.2889	1.7546
	50	2.9237	1.1964	3.3760	1.6656	2.9560	1.2485	3.3539	1.7309
	100	2.9274	1.1939	3.4026	1.6631	2.9632	1.2464	3.3868	1.7293
	150	2.9362	1.1916	3.4384	1.6611	2.9724	1.2435	3.4240	1.7269
	200	2.9465	1.1885	3.4757	1.6582	2.9817	1.2401	3.4619	1.7239
	300	2.9653	1.1820	3.5516	1.6519	2.9981	1.2313	3.5353	1.7150
$\langle 111\rangle$	0	2.6590	2.0269	2.0269	2.1712	2.7144	2.0354	2.0354	2.1868
	50	2.6694	2.0679	2.0679	2.2086	2.7171	2.0662	2.0662	2.2143
	100	2.6674	2.0819	2.0819	2.2204	2.7179	2.0836	2.0836	2.2297
	150	2.6692	2.1010	2.1010	2.2370	2.7196	2.1032	2.1032	2.2470
	200	2.6709	2.1208	2.1208	2.2542	2.7214	2.1231	2.1231	2.2645
	300	2.6752	2.1611	2.1611	2.2890	2.7223	2.1614	2.1614	2.2974

Table 4 predicts that the longitudinal ultrasonic velocities for PbX dominate the shear velocities, suggesting that the compressional mode plays a key role in ultrasonic wave propagation. The longitudinal velocity for PbS is highest at 300 K and occurs along the along $\langle 100\rangle$ direction and remains almost constant along the $\langle 111\rangle$ direction in the 0-300 K temperature regime due to the dependence of velocity on the second order elastic constants. The shear velocity V_{S2} due to transverse propagation is highest for PbS with $\langle 110\rangle$ at 300 K. The Debye velocity is increasing with temperature, when the wave is propagating in $\langle 111\rangle$ direction and decreasing with temperature for other two directions of propagation for both PbS and PbSe. Pei and Liu [45] reported the longitudinal, transverse and average velocity for PbS 4.08×10^3 ms^{-1}, 1.84×10^3 ms^{-1}, 2.04×10^3 ms^{-1} respectively at 300K and for PbSe 3.82×10^3 ms^{-1}, 1.72×10^3 ms^{-1}, 1.91×10^3 ms^{-1} respectively at 300K. The obtained longitudinal, shear and Debye average velocities for PbS for ultrasonic wave propagating in $\langle 100\rangle$ direction is 3.70×10^3 ms^{-1}, 1.18×10^3 ms^{-1}, 1.34×10^3 ms^{-1} respectively and for PbSe is 3.70×10^3 ms^{-1}, 1.23×10^3 ms^{-1}, 1.40×10^3 ms^{-1} respectively at 300K. Hence the present investigated values of the wave velocities are comparable with the previous findings reported experimentally [45]. The slight variations in the wave velocities of present investigations observed may be due to the consideration of wave propagation in all three directions along the $\langle 100\rangle, \langle 110\rangle$and $\langle 111\rangle$ direction, with the direction of polarization along $\langle 100\rangle, \langle 001\rangle, \langle 1\bar{1}0\rangle$ and $\langle \bar{1}10\rangle$, however experimentally reported data have not considered the same and may also involve experimental errors during the measurement process.

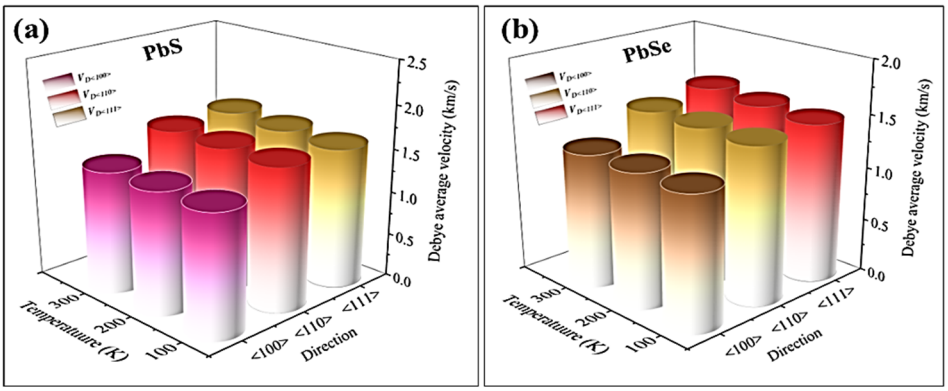

Figure 7. Debye average velocity in 100-300K temperature range along $\langle 100\rangle, \langle 110\rangle$ and $\langle 111\rangle$ for (a) PbS (b) PbSe

Table 4 and Fig.7 show that the Debye mean velocities are highest in the $\langle 111\rangle$ and lowest in the $\langle 100\rangle$ direction respectively. The Debye characteristic temperature of a solid material provides details about the vibration spectrum, elastic properties and thermodynamic properties of the material. It is the highest normal mode of oscillation of a

crystalline material and combines elastic properties such as thermal expansion, phonon dispersion, specific heat, thermal conductivity and lattice enthalpy [42]. The Debye temperature, as a bridge between elastic and thermal properties, is calculated by Eq. (5). The Debye temperature for PbS and PbSe is shown in Figures 8,9.

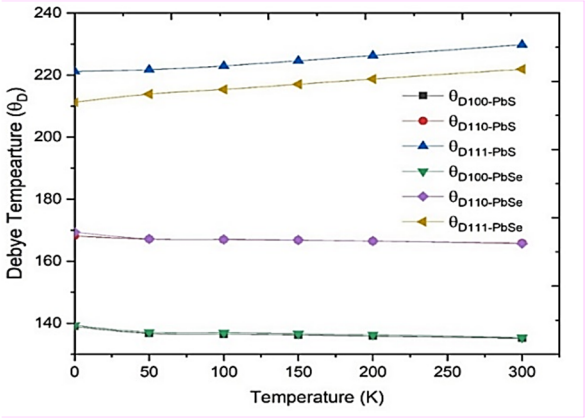

Figure 8. Debye temperature along ⟨100⟩, ⟨110⟩ and ⟨111⟩ for (a) PbS (b) PbSe

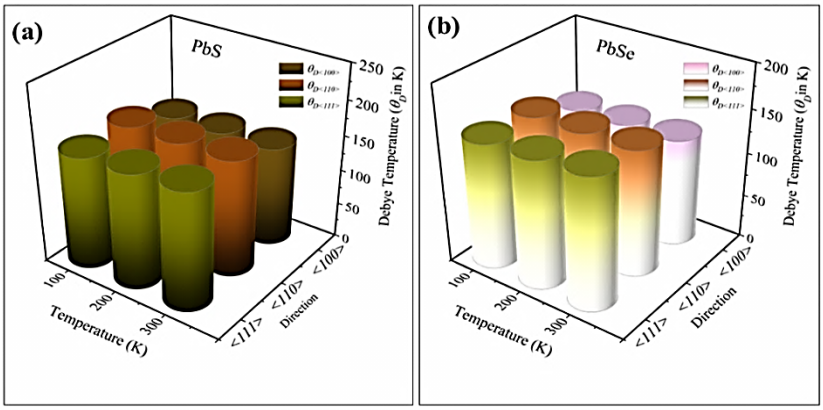

Figure 9. Debye average temperature in 100-300K temperature range along ⟨100⟩, ⟨110⟩ and ⟨111⟩ for (a) PbS (b) PbSe

Figure 9 shows that the Debye characteristic temperature for PbSe is lower than that for PbS because θ_D is inversely proportional to the cube of the molecular weight. The decreasing value of the Debye temperature as temperature increases is due to its dependence on the Debye velocity, which is a function of the second-order elastic constant. The Debye characteristic temperature is highest in the ⟨111⟩ direction, while it is lowest in the ⟨100⟩ direction for PbX. The Debye mean velocity is used to calculate the Debye characteristic temperature, which is used to estimate the thermal conductivity. The thermal conductivity is then used to calculate the thermal relaxation time, which is further used to calculate the nonlinearity parameter (acoustic coupling constant) and acoustic attenuation. The calculated values of thermal conductivity, nonlinearity parameter, and attenuation for PbS and PbSe are given in Tables 5 and 6, respectively. The thermal relaxation time along three crystallographic directions ⟨100⟩, ⟨110⟩ and ⟨111⟩ at 300K for PbS and PbSe is shown in Fig. 10.

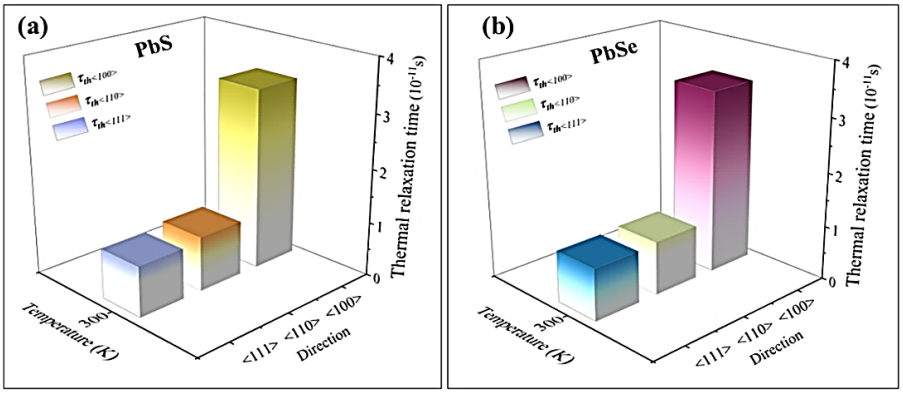

Figure 10. Thermal relaxation time at 300K along ⟨100⟩, ⟨110⟩ and ⟨111⟩ for (a) PbS (b) PbSe

Thermal conductivity is an indicator of thermal performance that is highest for PbS along the ⟨110⟩ direction at 300K. Thus, PbS along ⟨110⟩ has better thermal behavior than PbSe. Ultrasonic wave propagation through the material causes distortion in the phonon distribution. Wei et. al [46] reported the lattice thermal conductivity for PbS as 2.19 W/mK, while experimentally reported values are 2.52 W/mK, 2.38 W/mK, and 2.56 W/mK, respectively [45,47,48]. As depicted in Table 5, the thermal conductivity for PbS at 300 K under the present investigation is 3.84, 4.87, and 4.43 along the ⟨100⟩, ⟨110⟩ and ⟨111⟩ direction of wave propagation, respectively.

Table 5. κ(w/mK), D_L, D_{S1}, D_{S2}, $(\frac{\alpha}{\nu^2})_{th}$, $(\frac{\alpha}{\nu^2})_l$, $(\frac{\alpha}{\nu^2})_{S1}$, $(\frac{\alpha}{\nu^2})_{S2}$, $(\frac{\alpha}{\nu^2})_{total}$ ($\times 10^{-17}$ Nps^{2}m^{-1}) for PbS

Direction	Temp.	κ	D_L	D_{S1}	D_{S2}	$(\frac{\alpha}{\nu^2})_{th}$	$(\frac{\alpha}{\nu^2})_l$	$(\frac{\alpha}{\nu^2})_{S1}$	$(\frac{\alpha}{\nu^2})_{S2}$	$(\frac{\alpha}{\nu^2})_{total}$
⟨100⟩	50	3.78	32.12	1.023	1.023	0.01	16.79	7.166	7.166	31.141
	100	3.79	31.95	1.023	1.023	0.03	46.66	20.41	20.41	87.515
	150	3.80	31.39	1.022	1.022	0.04	77.38	35.36	35.36	148.14
	200	3.81	30.82	1.022	1.022	0.05	108.36	51.93	51.93	212.27
	300	3.84	29.74	1.021	1.021	0.07	163.64	86.38	86.38	336.47
⟨110⟩	50	4.74	39.85	0.622	62.77	0.16	28.57	3.257	14.61	46.593
	100	4.74	40.58	0.621	62.05	0.32	84.82	9.571	41.29	136.00
	150	4.79	40.32	0.619	61.28	0.45	147.05	16.90	69.59	233.99
	200	4.81	39.92	0.618	60.63	0.56	211.71	24.95	97.86	335.08
	300	4.87	39.07	0.615	59.62	0.73	342.60	42.58	152.16	538.07
⟨111⟩	50	4.30	28.19	40.23	40.23	0.33	11.67	17.91	17.91	47.823
	100	4.32	29.49	39.77	39.77	0.64	35.86	50.86	50.86	138.22
	150	4.35	29.18	39.26	39.26	0.92	63.28	87.29	87.29	238.78
	200	4.37	28.50	38.83	38.83	1.18	90.57	123.25	123.25	338.25
	300	4.43	26.91	38.13	38.13	1.64	141.83	190.62	190.62	524.71

Table 6. κ(w/mK), D_L, D_{S1}, D_{S2}, $(\frac{\alpha}{\nu^2})_{th}$, $(\frac{\alpha}{\nu^2})_l$, $(\frac{\alpha}{\nu^2})_{S1}$, $(\frac{\alpha}{\nu^2})_{S2}$, $(\frac{\alpha}{\nu^2})_{total}$ ($\times 10^{-17}$ Nps^{2}m^{-1}) for PbSe

Direction	Temp.	κ	D_L	D_{S1}	D_{S2}	$(\frac{\alpha}{\nu^2})_{th}$	$(\frac{\alpha}{\nu^2})_l$	$(\frac{\alpha}{\nu^2})_{S1}$	$(\frac{\alpha}{\nu^2})_{S2}$	$(\frac{\alpha}{\nu^2})_{total}$
⟨100⟩	50	3.56	30.84	1.003	1.003	0.016	20.36	7.801	7.801	35.978
	100	3.57	30.68	1.003	1.003	0.031	34.88	15.05	15.05	65.013
	150	3.58	29.53	1.002	1.002	0.043	59.00	24.83	24.83	108.71
	200	3.59	28.97	1.002	1.002	0.052	82.20	36.34	36.34	154.93
	300	3.61	27.92	1.001	1.001	0.067	125.16	61.12	61.12	247.46
⟨110⟩	50	4.43	36.88	0.619	58.61	0.1441	20.767	2.315	11.29	34.522
	100	4.45	39.54	0.618	57.74	0.2731	35.051	19.76	92.03	147.12
	150	4.47	37.37	0.616	56.92	0.3837	106.68	12.01	53.15	172.22
	200	4.50	36.96	0.614	56.20	0.4784	153.49	17.71	74.54	246.23
	300	4.55	36.15	0.610	55.11	0.6267	248.25	30.25	115.3	394.51
⟨111⟩	50	4.01	27.02	37.73	37.73	0.2582	9.3199	14.79	14.79	39.170
	100	4.03	31.40	37.17	37.17	0.4989	19.763	153.0	153.0	90.869
	150	4.05	27.99	36.65	36.65	0.7197	51.832	73.36	73.36	199.27
	200	4.08	27.34	36.18	36.18	0.9219	74.480	103.7	103.7	282.96
	300	4.12	25.75	35.45	35.45	1.283	112.46	154.7	154.7	423.14

The thermal relaxation time, τ_{th} for PbS and PbSe is of the order of 10^{-11} second, which confirms the semiconducting nature of the chosen materials [49]. τ_{th} is shortest along ⟨110⟩ and the highest along ⟨111⟩ as shown in Fig. 10, from which it can be inferred that the change in thermal energy to recover the phonon shape is faster along the ⟨110⟩ direction. The non-linearity parameter i.e. acoustic coupling constant is the parameter that quantifies the conversion of acoustic energy into thermal energy via the phonon interaction mechanism. The longitudinal coupling constant is higher in the ⟨110⟩ direction at 100K while the shear coupling constant is higher in the ⟨111⟩direction at 50K. The total coupling constant sum of longitudinal and shear coupling constants, is highest in the ⟨110⟩ direction, from which it can be inferred that the conversion of thermal to acoustic energy is highest in the ⟨110⟩ direction. The higher value of the coupling constant of PbS compared to PbSe shows that the conversion rate from thermal to acoustic energy is higher for PbS than for PbSe. It is clear from Table 5 that the loss due to the phonon-phonon (p-p) viscous process (Akheizer loss) dominates the thermal loss. The Ultrasonic attenuation due to the thermoelastic relaxation process is inversely proportional to the acoustic velocity [50].

Tables 5 and 6 clearly shows that ultrasonic attenuation caused by the thermoelastic relaxation mechanism is minimal compared to that from p-p interaction. This indicates that most of the ultrasonic energy loss happens as the system reaches equilibrium among different phonon branches and wave propagation directions. The similar values for ultrasonic attenuation among different directions of wave propagation reported previously [51] validate our findings and the approach we performed. The acoustic attenuation due to the thermoelastic relaxation process is largest in the ⟨111⟩ direction and smallest in the ⟨100⟩ direction for PbS and PbSe. The Akheizer damping at 300K is larger in the ⟨111⟩

direction and smaller in the ⟨100⟩ direction. Ultrasonic attenuation refers to the loss of energy in ultrasonic waves as they propagate through a material. It provides information on the microstructure, particle size, porosity, stress state and heterogeneity of the material. The total ultrasonic attenuation of PbS and PbSe is shown in Fig. 11 in the ⟨100⟩, ⟨110⟩ and ⟨111⟩ directions.

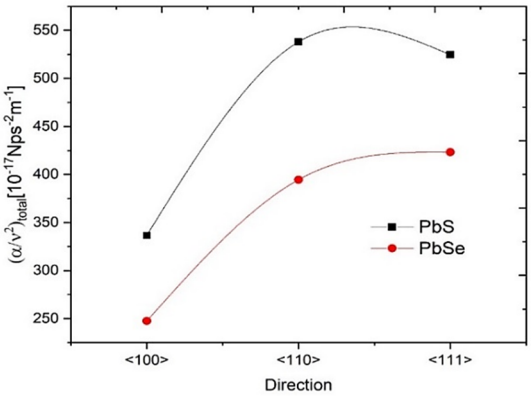

Figure 11. Total attenuation of PbS and PbSe along <100>, <110>, <111> direction

Figure 11 shows that PbS has higher attenuation values than PbSe, which imposes limitations on the applications of PbS. The ultrasonic attenuation coefficient shows that PbS is more suitable for applications that require minimal signal loss, such as in ultrasonic transducers and sensors. PbSe with large attenuation is used for applications where controlled energy dissipation is beneficial.

4. CONCLUSIONS

The Born potential model has been successfully applied to calculate the second- and third-order elastic constants and compared with existing results to validate the theory. The elastic constants are highest for PbSe indicating that PbSe is highly elastically stable. Pugh index, Cauchy pressure and Poisson ratio confirm that PbS and PbSe are brittle in nature in the temperature range 0-300 K. Zener anisotropy index indicates that PbS and PbSe are anisotropic. The thermal performance of PbS is better due to higher values of thermal conductivity and Debye temperature. The relaxation time is of the order of 10^{-11} second which validates the semiconducting nature of PbS and PbSe in the temperature range 0- 300K and in ⟨100⟩, ⟨110⟩ and ⟨111⟩ direction. The thermal energy to acoustic energy conversion is highest in the ⟨111⟩ direction for PbX. The attenuation coefficient of PbS is lower than that of PbSe. The total attenuation for both PbS and PbSe is the lowest in the⟨100⟩ direction, indicating that the ⟨100⟩ direction is the most suitable direction for wave propagation. These results offer a baseline for designing and improving PbX-based thermoelectric materials, sensors, and non-destructive ultrasonic evaluation systems.

Acknowledgements

The authors (PS, AS, DS) thank the Department of Science and Technology, New Delhi for providing support under DST-PURSE scheme (SR/PURSE/2024/230) to V.B.S. Purvanchal University, Jaunpur, Uttar Pradesh. Author Bin-Omran acknowledges the ongoing research funding program (ORF-2026-82), King Saud University, Riyadh, Saudi Arabia. For the purpose of open access, the author(s) have applied a Creative Commons Attribution (CC-BY) license to any Author Accepted Manuscript version arising from this submission.

ORCID

Sudhanshu Tripathi, https://orcid.org/0000-0001-8865-7987; **Praveen Singh,** https://orcid.org/0009-0006-7119-9119;
Anurag Singh, https://orcid.org/0009-0001-3877-9510; **Devraj Singh,** https://orcid.org/0000-0002-3011-2375;
R. Khenata, https://orcid.org/0000-0002-5573-1711; **M. Boudjelal,** https://orcid.org/0000-0001-6844-3789;
H. Meradji, https://orcid.org/0000-0002-3359-3725; **Ajit Kumar Maddheshiya,** https://orcid.org/0009-0005-0225-9387;
Shanay Rab, https://orcid.org/0000-0003-1203-6492; **M. Faizan,** https://orcid.org/0000-0003-1600-5095;
S. Bin-Omran, https://orcid.org/0000-0001-6097-2344

REFERENCES

[1] N. M. Ravindra, and V.K. Srivastava, "Properties of PbS, PbSe, and PbTe," Physica Status Solidi (a), **58**(1), 311(1980). https://doi.org/10.1002/pssa.2210580139

[2] Y. Zhang, X. Ke, C. Chen, J. Yang, and P.R.C. Kent, "Thermodynamic properties of PbTe, PbSe, and PbS: First-principles study," Physical Review B, **80**(2), 024304 (12 pp.) (2009). https://doi.org/10.1103/PhysRevB.80.024304

[3] L.D. Zhao, S.H. Lo, J. He, H. Li, K. Biswas, J. Androulakis, C.I. Wu, T.P. Hogan, D.Y. Chung, V.P. Dravid, and M.G. Kanatzidis, "High performance thermoelectrics from earth-abundant materials: Enhanced figure of merit in PbS by second phase nanostructures," Journal of the American Chemical Society, **133**(50), 20476–20487 (2011). https://doi.org/10.1021/ja208658w

[4] K. Biswas, J. He, I.D. Blum, C. I Wu, T.P.Hogan, D.N.Seidman, V.P. Dravid, and M.G. Kanatzidis, "High-performance bulk thermoelectrics with all-scale hierarchical architectures," Nature, **489**(9), 414-418 (2012). https://doi.org/10.1038/nature11439

[5] Kang, and F.W. Wise, "Electronic structure and optical properties of PbS and PbSe quantum dots," Journal of the Optical Society of America B, **14**(7), 1632-1646 (1997). https://doi.org/10.1364/JOSAB.14.001632
[6] S. Tripathi, R. Agarwal, and D. Singh, "Nonlinear elastic, ultrasonic and thermophysical properties of lead telluride," International Journal of Thermophysics, **40**(8), 78 (2019). https://doi.org/10.1007/s10765-019-2539-8
[7] Zair, B. E. Nabil Brahmi, and S. Bekhechi, "Structural, electronic and thermoelectric properties of PbS, PbSe and their ternary alloy $PbSe_{1-x}S_x$," International Journal of Modern Physics C, **34**(10), 2350130 (2023). https://doi.org/10.1142/S0129183123501309
[8] P. Priyadarshini, D. Sahoo, and R. Naik, "A review on the optical properties of some germanium-based chalcogenide thin films and their applications," Optical and Quantum Electronics, **54**(3), 166191 (2022). https://doi.org/10.1007/s11082-022-03564-4
[9] J. M. Skelton, S. C. Parker, A. Togo, I. Tanaka, and A. Walsh, "Thermal physics of the lead chalcogenides PbS, PbSe, and PbTe from first principles," Physical Review B, **89**(20), 205203 (2014). https://doi.org/10.1103/PhysRevB.89.205203
[10] S. Anwar, S. Anwar, and B. K. Mishra, "Effect of bath temperature on PbSe thin films prepared by chemical synthesis," Materials Science in Semiconductor Processing, **40**(Dec. 2015), 910-916 (2015). https://doi.org/10.1016/j.mssp.2015.07.077
[11] X. Chen, Y. B. Zhu, Z. Xing, G. Tang, and H. Fan, "Synthesis of PbSe nanostructures with different size and morphology and their electrochemical properties," Journal of Materials Science: Materials in Electronics, **27**(10), 1151–1157 (2016). https://doi.org/10.1007/s10854-015-3864-8
[12] H.D. Jahromi, and M. Moaddeli, "Lead sulfide: a new candidate for optoelectronics applications in the ultraviolet spectral range," Materials Research Express, **6**(11), 116220 (2019). https://doi.org/10.1088/2053-1591/ab513d
[13] S. Abe, "Phase transformation from PbS to PbSe: S in hot-wall deposition of nanocomposite thin film with evaporation sources of PbS and ZnSe," Discover Applied Sciences, **3**(1), 212 220 (2021). https://doi.org/10.1007/s42452-021-04236-w
[14] C.K. Bandoh, I. Nkrumah, F.K. Ampong, R.K. Nkrumah, and F. Boakye, "Effect of annealing on the structure and optical properties of lead selenide and cadmium selenide thin film prepared by chemical bath deposition," Chalcogenide Letters, **18**(2), 81-89 (2021). https://doi.org/10.15251/CL.2021.182.81
[15] B. Batu and T. Tamasgen, "Effects of thickness on optical and structural properties of lead sulfide (PbS) thin film prepared by chemical bath deposition," Journal of Natural Sciences Research, **13**(9), 1-6 (2022). https://doi.org/10.7176/JNSR/13-9-01
[16] N. Khusayfan, H. Khanfar, and R.N. Alharbi, Fabrication and characterization of lead selenide thin film as X-ray sensors, photovoltaic devices and microwave resonators," Applied Physics A, **129**(9), 639 (8 pp.) (2023). https://doi.org/10.1007/s00339-023-06909-2
[17] C. Yang, X. Zhang X, P. Li, S. Chen, and S. Feng, "Electrochemical synthesis of hierarchical porous PbSe film and its infrared photodetection properties," Applied Surface Science, **663**, 160145 (2024). https://doi.org/10.1016/j.apsusc.2024.160145
[18] K. Brugger, "Thermodynamic definition of higher order elastic coefficients," Physical Review, **133,** A1611-A1612 (1964). https://doi.org/10.1103/PhysRev.133.A1611
[19] G. Leibfried, and W. Ludwig, "Theory of anharmonic effects in crystals," in: *Solid State Physics*, vol. 12, edited by F. Seitz, and D. Turnbull (Academic Press, New York, 1961), pp. 275-444. https://doi.org/10.1016/S0081-1947(08)60656-6
[20] P.B. Ghate, "Third order elastic constants of alkali halide crystals," Physical Review, **139**(5A)**,** A1666-A1674 (1965). https://doi.org/10.1103/PhysRev.139.A1666
[21] S. Mori, and Y. Hiki, "Calculation of the third- and fourth-order elastic constants of alkali halide crystals," Journal of the Physical Society of Japan, **45**(5), 1449-1456 (1978). https://doi.org/10.1143/JPSJ.45.1449
[22] J. Bala, S.P. Singh, A.K. Verma, D.K. Singh, and D. Singh, "Elastic, mechanical and ultrasonic studies of boron monopnictides in two different structural phases," Indian Journal of Physics, **96**(11), 3191-3200 (2022). https://doi.org/10.1007/s12648-021-02278-9
[23] S. Tripathi, R. Agarwal, and D. Singh, "Elastic, mechanical and ultrasonic properties of nanostructured IIIrd group phosphides," MAPAN – Journal of Metrology Society of India, **36**(1), 97–107 (2021). https://doi.org/10.1007/s12647-020-00412-2
[24] Singh, and D. Singh, "Investigation of alkali halide crystals AX (A = Li, Na, K; X = F, Cl, Br) by elastic, mechanical and ultrasonic analysis," Zeitschrift für Naturforschung A, **78**(10), 947-958 (2023). https://doi.org/10.1515/zna-2023-0138
[25] Cz. Jasiukiewicz, and V. Karpus, "Debye temperature of cubic crystals," Solid State Communications, **128**(5), 167-169 (2003), https://doi.org/10.1016/j.ssc.2003.08.008
[26] C. Tripathy, D. Singh, and R. Paikaray, "Behaviour of elastic and ultrasonic properties of curium monopnictides," Canadian Journal of Physics, **96**(5), 513-518 (2018). https://doi.org/10.1139/cjp-2017-0491
[27] J. Bala, and D. Singh, Elastic and ultrasonic properties of fermium monopnictides," Engineering and Applied Science Research, **47**(2), 182-189 (2020). https://ph01.tci-thaijo.org/index.php/easr/article/view/216247
[28] D.E. Gray, *American Institute of Physics Handbook*, 3rd ed. (McGraw-Hill, New York, 1972).
[29] D. Singh, "Behaviour of acoustic attenuation in rare-earth chalcogenides," Materials Chemistry and Physics, **115**(1), 65-68 (2009). https://doi.org/10.1016/j.matchemphys.2008.11.025
[30] Y. I. Hwang, D. Sung, H.J. Kim, S. J. Song, K. B. Kim, and S. S. Kang, "Propagation and attenuation characteristics of an ultrasonic beam in dissimilar metal welds," Sensors, **20**(21), 6259-6276 (18 pp.) (2020). https://doi.org/10.3390/s20216259
[31] W. P. Mason, Effect of impurities phonons processes on the ultrasonic attenuation of germanium crystal, quartz and silicon, In: *Physical Acoustics. vol III B*, edited by W. P. Mason (Academic Press, New York, 1965), pp 237-286. https://doi.org/10.1016/B978-0-12-395669-9.50013-8
[32] D. Singh, A. Kumar, V. Bhalla, and R. K. Thakur, "Mechanical and thermophysical properties of actinide monocarbides," Modern Physics Letters B, **32**(21), 1850248 (2018). https://doi.org/10.1142/S0217984918502482
[33] D. Singh, D.K. Pandey, D. K. Singh, and R.R. Yadav, "Propagation of ultrasonic waves in neptunium monochalcogenides," Applied Acoustics, 72(10), 737-741 (2011). https://doi.org/10.1016/j.apacoust.2011.04.002
[34] E.M. El-Menyawy, G.M. Mahmoud, R.S. Ibrahim, F.S. Terra, H. El-Zahed, and I.K. El Zawawi, "Structural, optical and electrical properties of PbS and PbSe quantum dot thin films," Journal of Materials Science: Materials in Electronics, **27**(10), 10070-10077 (2016). https://doi.org/10.1007/s10854-016-5080-6
[35] M.P. Tosi, Cohesion of ionic solids in the Born model, In: *Solid State Physics, vol 16*, edited by F. Seitz, and D. Turnbull (Academic Press, New York, 1961), pp. 1–120. https://doi.org/10.1016/S0081-1947(08)60515-9
[36] J.F. Nye, *Physical Properties of Crystals: Their Representation by Tensors and Matrices*. (Oxford University Press, New York 1985).

[37] C.S.G. Cousins, "New relations between elastic constants of different orders under central force interactions," Journal of Physics C: Solid State Physics, **4**(10), 1117-1123 (1971). https://doi.org/ 10.1088/0022-3719/4/10/020
[38] A. Singh, S. Tripathi, and D. Singh, "Elastic, thermophysical and ultrasonic investigation of tin monochalcogenides," Modern Physics Letters B, **38**(32), 2450280 (2024). https://doi.org/10.1142/S0217984924502804
[39] O. Madelung, M. Schulz, and H. Weiss, editors, *Numerical Data and Functional Relationships in Science and Technology Landolt-Bornstei, New Series,* vol. 17, (Springer, Berlin, 1983).
[40] H. Takia, M.A. Rahman, R. Moshiur, M.M. Rahaman, and K. Hossen, "The substantive characteristics of layered PbX (X= S, Se, and Te) compounds: An ab-inito investigations," International Journal of Physics, **10**(2), 102-110 (2022). https://doi.org/10.12691/ijp-10-2-3
[41] T. Seetawan, and H. Wattanasarn, "First principle simulation mechanical properties of PbS, PbSe, CdTe and PbTe by molecular dynamics," Procedia Engineering, **32**, 609-613 (2012). https://doi.org/10.1016/j.proeng.2012.01.1316
[42] P. Ravindran, L. Fast, P. Korzhavyi, B. Johansson, J. Wills and O. Eriksson, "Density functional theory for calculation of elastic properties of orthorhombic crystals: Application to $TiSi_2$," Journal of Applied Physics, **84**(9), 4891(1998). https://doi.org/10.1063/1.368733
[43] H. Ozisik, E. Deligoz, G. Surucu, and H.B. Ozisik, Anisotropic elastic and vibrational properties of Ru_2B_3 and Os_2B_3: a first-principles investigation," Materials Research Express, **3**(7), 076501 (2016). https://doi.org/10.1088/2053-1591/3/7/076501
[44] Kumar, "Ultrasonic velocity ratio: An effective tool for in-situ materials characterization," Acta Acustica united with Acustica, **104**(2), 251-258 (2018). https://doi.org/10.3813/AAA.919167
[45] Y. L. Pei, and Y. Liu, "Electrical and thermal transport properties of Pb-based chalcogenides: PbTe, PbSe, and PbS," Journal of Alloys and Compounds, **514**(2), 40-44(2012). https://doi.org/10.1016/j.jallcom.2011.10.036
[46] L. Wei, J. F. Chen, Q. Y. He, and W. Teng, "Study of lattice thermal conductivity of PbS," Journal of Alloys and Compounds, **584**(1), 381-384 (2014). https://doi.org/10.1016/j.jallcom.2013.09.081
[47] S. Johnsen, J. Q. He, J. Androulakis, V. P. Dravid, I. Todorov, D. Y. Chung, and M. G. Kanatzidis, "Nanostructures boost the thermoelectric performance of PbS," Journal of the American Chemical Society, **133**(10), 3460–3470 (2011). https://doi.org/10.1021/ja109138p
[48] L.D. Zhao, S.H. Lo, J.Q. He, H. Li, K. Biswas, J. Androulakis, C. Wu, *et al*., "High performance thermoelectrics from earth-abundant materials: Enhanced figure of merit in PbS by second phase nanostructures," Journal of the American Chemical Society, **133**(50), 20476–20487 (2011). https://doi.org/10.1021/ja208658w
[49] D. Singh, R.R. Yadav, and A.K. Tiwari, Ultrasonic attenuation in semiconductors," Indian Journal of Pure and Applied Physics, **40**(12), 845-849 (2002). https://nopr.niscpr.res.in/handle/123456789/26219
[50] K. Ono, "A comprehensive report on ultrasonic attenuation of engineering materials, including metals, ceramics, polymers, fiber-reinforced composites, wood, and rocks," Applied Sciences, **10**(7), 2239 (52 pp.) (2020). https://doi.org/10.3390/app10072230
[51] K.M. Raju, R.K. Srivastava, A. Kumar, and S. Devi, "Acoustical investigation of lead chalcogenides," Physica B: Condensed Matter, **405**(23), 4855-4857 (2010). https://doi.org/10.1016/j.physb.2010.09.018

НЕРУЙНУЮЧА УЛЬТРАЗВУКОВА ОЦІНКА ТЕМПЕРАТУРО-ЗАЛЕЖНИХ МЕХАНІЧНИХ І ПРУЖНИХ ВЛАСТИВОСТЕЙ СПОЛУК PbX (X = S, Se)

Судханшу Тріпаті[1], Правін Сінгх[2], Анураг Сінгх[2,3], Деврадж Сінгх[2], Р. Кхената[4,5], М. Буджелал[4], Х. Мераджи[6], Аджит Кумар Маддхешія[7], Шанай Раб[8], М. Файзан[9], С. Бін-Омран[10]

[1]Інститут інформаційних технологій Аміті, Університет Аміті, Сектор-125, Нойда – 201313, Уттар-Прадеш, Індія
[2]Кафедра фізики, Інститут фізичних наук ім. професора Раджендри Сінгха (Раджу Бхайя), Університет Вір Бахадур Сінгх Пурванчал, Джаунпур-222003, UP, Індія
[3]Факультет фізики, Державний коледж, Бабхані, Сонбхадра-231208, UP, Індія
[4]Лабораторія фізики квантової механіки та математичного моделювання (LPQ3M), Університет Маскара, Маскара, 29000, Алжир
[5]Алжирська академія наук і технологій, 04- Шлях світу, Гідра-Алжир16000, Алжир
[6]Лабораторія LPR, Департамент фізики, Факультет природничих наук, Університет Баджі Мохтар, Аннаба, Алжир
[7]Кафедра фізики Аллахабадського університету, Праяградж-211002, Індія
[8]Школа архітектури, технологій та інженерії, Брайтонський університет, BN24AT, Великобританія
[9]Школа матеріалознавства та інженерії Цзилінського університету, Чанчунь, 130012, Китай
[10]Кафедра фізики та астрономії, коледж науки, Університет короля Сауда, а/с 2455, Ер-Ріяд, 11451, Саудівська Аравія

Проведено всебічне дослідження пружних, механічних та термоакустичних властивостей монохалькогенідів свинцю PbX (X = S, Se) вздовж основних кристалографічних напрямків ⟨100⟩, ⟨110⟩ та ⟨111⟩ у діапазоні температур 0–300 K з використанням ультразвукового неруйнівного методу оцінки. Пружні постійні другого та третього порядку (SOEC та TOEC) були розраховані з використанням кулонівської та борнівсько-майєрівської потенційних моделей, що підтверджують пружну стабільність досліджуваних матеріалів. Похідні механічні параметри та швидкості ультразвуку були отримані з SOEC, що вказує на тендітну механічну поведінку, засновану на коефіцієнті Кнута. При температурі 300 K були визначені температура Дебая, швидкість Дебая, теплопровідність грат, параметр акустичної нелінійності та коефіцієнт ультразвукового згасання вздовж досліджуваних напрямків. Серед усіх напрямків орієнтація ⟨111⟩ показала найвищу температуру Дебая та швидкість Дебая. Домінуючим механізмом ультразвукового згасання було ідентифіковано механізм типу Ахіезера, що підкреслює його роль у тепловіддачі та акустичному демпфуванні. Результати показують, що PbSe має чудову пружну жорсткість, тоді як PbS демонструє підвищену теплопровідність і сильніші фононні взаємодії. Ці характеристики підкреслюють потенціал PbS та PbSe для застосування в термоелектричних і ультразвукових сенсорних технологіях.

Ключові слова: *монохалькогеніди свинцю; пружні властивості; механічні константи; теплопровідність; ультразвукове згасання*